

# Long-Term Auto-Regressive Prediction using Lightweight AI Models: Adams-Bashforth Time Integration with Adaptive Multi-Step Rollout

Sunwoong Yang<sup>a</sup>, Ricardo Vinuesa<sup>b</sup>, Namwoo Kang<sup>a,c,\*</sup>

<sup>a</sup>*Cho Chun Shik Graduate School of Mobility, Korea Advanced Institute of Science and Technology, Daejeon, 34051, Republic of Korea*

<sup>b</sup>*FLOW, Engineering Mechanics, KTH Royal Institute of Technology, Stockholm, SE-100 44, Sweden*

<sup>c</sup>*Narnia Labs, Daejeon, 34051, Republic of Korea*

---

## Abstract

This study addresses the critical challenge of error accumulation in spatio-temporal auto-regressive predictions within scientific machine learning models by introducing innovative temporal integration schemes and adaptive multi-step rollout strategies. We present a comprehensive analysis of time integration methods, highlighting the adaptation of the two-step Adams-Bashforth scheme to enhance long-term prediction robustness in auto-regressive models. Additionally, we improve temporal prediction accuracy through a multi-step rollout strategy that incorporates multiple future time steps during training, supported by three newly proposed approaches that dynamically adjust the importance of each future step. Despite using an extremely lightweight graph neural network with just 1,177 trainable parameters and training on only 50 snapshots, our framework accurately predicts 350 future time steps—a 7:1 prediction-to-training ratio—achieving an error of only 1.6% compared to the vanilla auto-regressive approach. Moreover, our framework demonstrates an 83% improvement in rollout performance over the standard noise injection method, a standard technique for enhancing long-term rollout performance. Its effectiveness is further validated in more challenging scenarios with truncated meshes, showcasing its adaptability and robustness in practical applications. This work introduces a versatile framework for robust long-term spatio-temporal auto-regressive predictions that shows potential for mitigating error accumulation across various model types and engineering disciplines.

*Keywords:* Spatio-temporal auto-regressive prediction, Scientific machine learning, Graph neural networks, Two-step Adams-Bashforth method, Adaptive multi-step rollout

---

## 1. Introduction

In the era of scientific machine learning (SciML), auto-regressive (AR) models have emerged as powerful tools for spatio-temporal prediction across various engineering disciplines, particularly in physical domains like fluid dynamics [1, 2, 3, 4, 5, 6]. They predict future states by recursively using their own previous predictions as inputs for subsequent forecasts—specifically, each new prediction becomes part of the input sequence for the next prediction step, creating a chain of sequential forecasts based on historical data. This recursive approach facilitates real-time forecasting and dynamic decision-making across a wide range of engineering applications [7, 8, 9, 10, 11, 12]. Unlike other emerging SciML approaches such as physics-informed neural networks or DeepONet, which incorporate the time coordinate directly into the input and therefore violate temporal causality [13, 14, 15], AR models predict future states based on past historical information. This sequential prediction aligns with the natural progression of physical processes, preserving causality by ensuring that each snapshot at a given time depends solely on preceding snapshots, without any influence from future information.

---

\*Corresponding author. [nwkang@kaist.ac.kr](mailto:nwkang@kaist.ac.kr)

*Email addresses:* [sunwoongy@kaist.ac.kr](mailto:sunwoongy@kaist.ac.kr) (Sunwoong Yang), [rvinuesa@mech.kth.se](mailto:rvinuesa@mech.kth.se) (Ricardo Vinuesa)

However, AR models have inherent limitations, most notably error accumulation during long-term rollouts [2, 16, 17, 18, 19]. Since each prediction depends on the previous output, any inaccuracies introduced at one step can propagate and amplify in subsequent steps, leading to significant deviations from the true physical behavior over time. Recent approaches attempt to address this limitation by combining data-driven models with traditional numerical solvers, using the latter to recalibrate data-driven predictions when SciML model errors exceed certain thresholds [20, 21]. However, such hybrid approaches significantly compromise the primary advantage of ML-based surrogate models, their real-time prediction capability, as demonstrated by insufficient speedup factors: for example, approximately 1.9 times acceleration compared to pure computational fluid dynamics (CFD) simulations [21]. This highlights the critical need for improving the long-term prediction accuracy of purely data-driven AR models while preserving their computational efficiency, enabling real-time predictions without relying on expensive numerical solver re-calibrations.

To enhance the robustness of AR-based spatio-temporal predictions over long-term rollouts, the most frequently used approach is noise injection, where noise is added to the input data during the training phase [17, 22, 23, 24]. This method deliberately perturbs the training inputs with random noise to simulate the prediction errors that naturally occur during rollout. By exposing the model to slightly corrupted inputs during training, it learns to handle imperfect data and becomes more robust when its own imperfect predictions are fed back as inputs during inference. However, noise injection requires careful tuning of the noise scale, which is highly data-dependent, and its stochastic nature can lead to inconsistent and unstable training process.

This study presents a novel framework for enhancing long-term auto-regressive (AR) predictions in resource-constrained environments through the integration of numerical time-integration schemes and adaptive multi-step rollout techniques. Our approach specifically addresses a critical challenge in scientific machine learning: achieving robust long-term predictive performance with limited training data and model capacity while maintaining real-time inference capabilities. Extensive experiments, including comparisons with traditional noise injection methods and evaluations under challenging mesh conditions, demonstrate our framework’s ability to achieve exceptional long-term stability and accuracy despite these constraints. Our key contributions can be summarized as follows:

1. **Assessment under challenging but practical conditions:** In real-world engineering scenarios, models often encounter challenging constraints such as limited availability of training data, restricted model capacity, and the need to handle varying mesh topologies arising from diverse shape configurations. To address these challenges, we develop a GNN-based AR model that achieves accurate long-term predictions of future states (up to 350 rollouts) using only 50 past snapshots, with a lightweight architecture containing only 1,177 trainable parameters. This demonstrates the feasibility of robust long-term prediction even under severe resource constraints that are common in practical applications.
2. **Comprehensive evaluation of time integration schemes for AR prediction:** For the first time in the context of AR prediction within SciML models, we comprehensively explore various time integration schemes, including direct prediction, forward Euler, second-order central difference, and two-step Adams-Bashforth methods. Through systematic evaluation, we demonstrate that the Adams-Bashforth scheme consistently outperforms other approaches, achieving a 7% improvement in prediction accuracy compared to the commonly used forward Euler method. While other schemes exhibit instability with increased multi-step rollout, Adams-Bashforth maintains robust performance across varying prediction horizons, even when the direct prediction approach fails to converge.
3. **Proposal of adaptive multi-step rollout strategies:** We introduce a novel concept of adaptive multi-step rollout to address limitations in conventional multi-step training approaches. By developing three adaptive weighting strategies that dynamically adjust the importance of different future time steps, we significantly enhance prediction stability. Our best approach, which emphasizes only the first and last future components, delivers an 89% improvement over conventional fixed-weight multi-step rollout and outperforms other adaptive strategies by up to 80%, while maintaining similar computational costs. This demonstrates the effectiveness of selectively emphasizing critical time steps during training.

4. **Comparison with noise-injection methods:** Our integration of the Adams-Bashforth method with adaptive multi-step rollout achieves an 83% improvement in prediction accuracy compared to conventional noise injection techniques—the current standard approach for enhancing long-term rollout stability. Our analysis reveals that combining multi-step rollout with noise injection degrades performance due to a previously unidentified negative interaction between these error-mitigation strategies.
5. **Robustness evaluation on a more challenging mesh:** Tests using a truncated mesh—where only a subset of the complete mesh containing all flow quantities is used for training—show that our method achieves 58% and 27% improvement over direct prediction and forward Euler approaches respectively. This demonstrates our framework’s applicability in scenarios where computational memory constraints necessitate focusing on specific regions of interest within complex flow fields.
6. **General applicability of the proposed approach:** We intentionally design our framework to be model-agnostic and application-independent, focusing on fundamental AR prediction mechanics rather than domain-specific features. This ensures our techniques can be seamlessly integrated with any AR model across diverse engineering disciplines without requiring specialized adaptations.

The remainder of this paper is organized as follows. Section 2 presents the theoretical framework of our proposed time integration schemes and adaptive multi-step rollout strategies. Section 3 details the overall experimental setup. Sections 4 and 5 demonstrate the effectiveness of time integration schemes and multi-step rollout techniques, respectively. Section 6 introduces our adaptive weighting approaches and analyzes their impact on prediction robustness. Section 7 provides comparative analysis with existing noise injection methods. Section 8 evaluates model performance under more challenging mesh conditions with truncated domains. Finally, Section 9 concludes the paper with discussions on broader implications and future research directions.

## 2. Methods: time integration schemes and adaptive multi-step rollout

### 2.1. Auto-regressive rollout with different time integration schemes

#### 2.1.1. Motivation

While advanced time-stepping schemes have been extensively studied in traditional CFD, their application in AI-driven flow prediction remains limited. Most AI-based temporal flow prediction research has focused only on direct prediction [1, 3, 4, 24] or simple forward Euler methods [2, 22, 23], leaving the potential impact of other finite difference schemes largely unexplored.

To address this gap, we investigate various numerical finite difference schemes for enhancing long-term AR prediction accuracy. Unlike traditional numerical analysis, where schemes are evaluated based on formal order-of-accuracy, AR models implicitly learn temporal dynamics from data. In our framework, each finite difference method computes the training target for temporal derivatives with inherently different structural biases—from simple first-order approximations in forward Euler to symmetric formulations in central difference schemes to the multi-step approach of Adams-Bashforth which incorporates richer temporal history.

This investigation represents the first comprehensive study to evaluate how different derivative approximation methods affect AR model’s ability to capture spatiotemporal dynamics in fluid flow prediction. The observed benefits with particular integration methods arise from favorable interplay between numerical approximation and the model’s data-driven learning process.

#### 2.1.2. Investigated time integration schemes

We explore three finite difference schemes (forward Euler, second-order central difference, and Adams-Bashforth) and compare them with conventional direct prediction. It’s important to note that the formal order-of-accuracy concept doesn’t directly translate to AR models, as they learn temporal dependencies implicitly rather than following fixed error bounds. Figure 1 visualizes model outputs across all schemes. The Runge-Kutta method, though widely used in CFD, is excluded due to its incompatibility with data-driven AR processes (details in Appendix A).

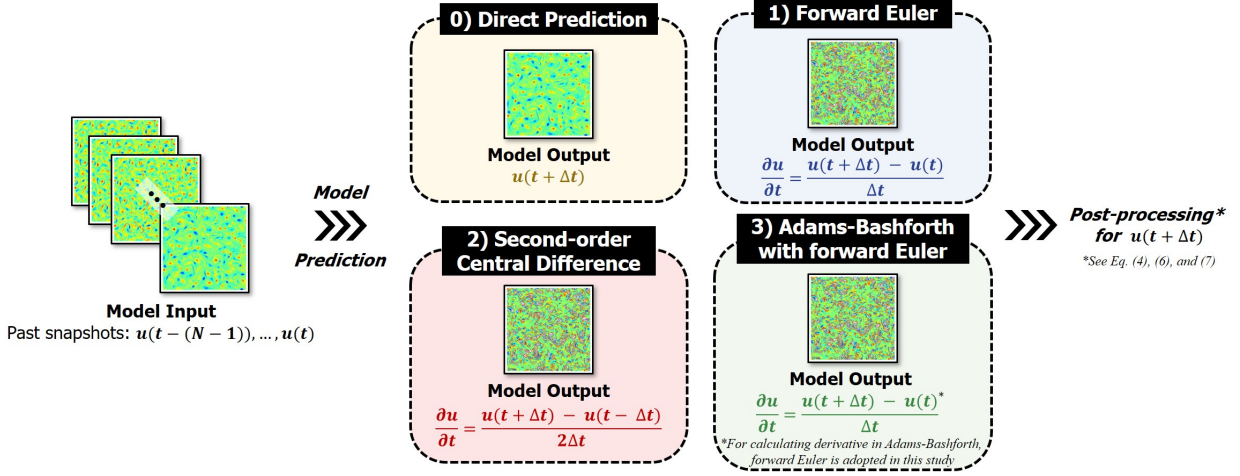


Figure 1: Overview of time integration schemes investigated in this study. While both forward Euler and Adams-Bashforth yield identical model predictions during simulation, they differ in how they compute the subsequent timestep  $u(t + \Delta t)$  during post-processing: forward Euler uses a single-step explicit update (Eq. 4), whereas Adams-Bashforth employs a two-step approach incorporating previous timesteps (Eq. 7).

**0) Conventional approach: direct prediction.** In the direct prediction approach, the AR model directly predicts the flow field at the next time step based on input from previous time steps:

$$\mathbf{u}(t + \Delta t) = AR \left( \underbrace{\mathbf{u}(t), \mathbf{u}(t - \Delta t), \dots, \mathbf{u}(t - (N - 1)\Delta t)}_{\text{past } N \text{ snapshots}} \right) \quad (1)$$

where  $\mathbf{u}(t)$  represents the flow field at time  $t$ ,  $\Delta t$  is the time step size,  $N$  is the number of past time steps used as input, and  $AR$  refers to the AR model with past  $N$  snapshots as inputs. Here, it is important to note that  $\Delta t = 1$  can be assumed since  $\Delta t$  represents the conceptual difference between successive snapshot datasets rather than an actual physical time interval [23]—therefore,  $\Delta t = 1$  is assumed for the simplicity throughout this study. Returning to the main point, this conventional approach does not explicitly leverage past snapshot datasets when predicting  $\mathbf{u}(t + \Delta t)$ , even though they are used as inputs to black-box AR models, ultimately reducing both training and inference efficiency.

**1) Forward Euler method.** Instead of predicting the next time step directly, forward Euler method [22, 25, 26, 27] makes the AR model predict the rate of change of the flow field,  $\frac{\delta \mathbf{u}}{\delta t}$ :

$$\frac{\delta \mathbf{u}}{\delta t} = AR(\mathbf{u}(t), \mathbf{u}(t - \Delta t), \dots, \mathbf{u}(t - (N - 1)\Delta t)) \quad (2)$$

where the rate of change is computed by:

$$\frac{\delta \mathbf{u}}{\delta t} = \frac{\mathbf{u}(t + \Delta t) - \mathbf{u}(t)}{\Delta t} \quad (3)$$

and therefore the next time step can be obtained as:

$$\mathbf{u}(t + \Delta t) = \mathbf{u}(t) + \Delta t \cdot \frac{\delta \mathbf{u}}{\delta t} \quad (4)$$

Before training, the label for  $\frac{\delta \mathbf{u}}{\delta t}$  is computed from the given data using the forward Euler method shown in Eq. 3, and AR model is trained to output the corresponding  $\frac{\delta \mathbf{u}}{\delta t}$  as in Eq. 2. During inference, the AR model predicts  $\frac{\delta \mathbf{u}}{\delta t}$  based on past flow fields, and finally  $\mathbf{u}(t + \Delta t)$  can be obtained as in Eq. 4.

2) **Second-order central difference.** With this scheme, the AR model again predicts the  $\frac{\delta \mathbf{u}}{\delta t}$  as in Eq. 2 but the term  $\frac{\delta \mathbf{u}}{\delta t}$  is defined with the form of second-order central difference [28] as:

$$\frac{\delta \mathbf{u}}{\delta t} = \frac{\mathbf{u}(t + \Delta t) - \mathbf{u}(t - \Delta t)}{2\Delta t} \quad (5)$$

and therefore the next time step can be obtained as:

$$\mathbf{u}(t + \Delta t) = \mathbf{u}(t - \Delta t) + 2\Delta t \cdot \frac{\delta \mathbf{u}}{\delta t} \quad (6)$$

This method considers both forward and backward time steps for the calculation of  $\frac{\delta \mathbf{u}}{\delta t}$ , potentially offering improved accuracy when flow properties vary smoothly over time. However, when the flow exhibits oscillatory behavior, this approach can lead to erratic predictions. Also, from Eq. 6, note that the next time step  $\mathbf{u}(t + \Delta t)$  is highly dependent on  $\mathbf{u}(t - \Delta t)$  without the intermediate time step  $\mathbf{u}(t)$ , which will be discussed later (Fig. 5 in Section 4.1).

3) **Adams-Bashforth with forward Euler (Adams-Euler).** Next, we explore the two-step Adams-Bashforth method, which again requires derivative information for prediction. The general form of the Adams-Bashforth update is:

$$\mathbf{u}(t + \Delta t) = \mathbf{u}(t) + \Delta t \cdot \left( \frac{3}{2} \frac{\delta \mathbf{u}}{\delta t} \Big|_t - \frac{1}{2} \frac{\delta \mathbf{u}}{\delta t} \Big|_{t-\Delta t} \right) \quad (7)$$

where  $\frac{\delta \mathbf{u}}{\delta t} \Big|_t$  represents the rate of change of  $\mathbf{u}$  at the current timestep and  $\frac{\delta \mathbf{u}}{\delta t} \Big|_{t-\Delta t}$  denotes the rate of change at the previous timestep.

A critical aspect of implementing the Adams-Bashforth method in an AR framework is the choice of how to approximate the derivatives  $\frac{\delta \mathbf{u}}{\delta t} \Big|_t$  and  $\frac{\delta \mathbf{u}}{\delta t} \Big|_{t-\Delta t}$ . We implement the forward Euler method for time integration (Eq. 8 and Eq. 9), a common approach in AI-based temporal prediction [2, 22, 23]. Since both methods employ the forward Euler scheme to compute the derivatives, the forward Euler and Adams-Bashforth approaches yield identical model outputs: see Eq. 1 and Eq. 8. For brevity, we refer to the combined Adams-Bashforth with forward Euler method as ‘‘Adams-Euler’’ throughout this paper.

$$\frac{\delta \mathbf{u}}{\delta t} \Big|_t = \frac{\mathbf{u}(t + \Delta t) - \mathbf{u}(t)}{\Delta t} = AR \left( \underbrace{\mathbf{u}(t), \mathbf{u}(t - \Delta t), \dots, \mathbf{u}(t - (N - 1)\Delta t)}_{\text{past } N \text{ snapshots from } t} \right) \quad (8)$$

$$\frac{\delta \mathbf{u}}{\delta t} \Big|_{t-\Delta t} = \frac{\mathbf{u}(t) - \mathbf{u}(t - \Delta t)}{\Delta t} = AR \left( \underbrace{\mathbf{u}(t - \Delta t), \mathbf{u}(t - 2\Delta t), \dots, \mathbf{u}(t - N\Delta t)}_{\text{past } N \text{ snapshots from } (t - \Delta t)} \right) \quad (9)$$

The Adams-Euler method thus comprises two main components:

1. **Forward Euler derivative approximation:** We compute the derivatives  $\frac{\delta \mathbf{u}}{\delta t} \Big|_t$  and  $\frac{\delta \mathbf{u}}{\delta t} \Big|_{t-\Delta t}$  using the forward Euler method (Eqs. 8 and 9). This approach is consistent with previous AR studies and provides a straightforward and effective means to compute derivatives, which will be used as training labels [22, 23].
2. **Two-step Adams-Bashforth integration:** The update in Eq. 7 utilizes both  $\frac{\delta \mathbf{u}}{\delta t} \Big|_t$  and  $\frac{\delta \mathbf{u}}{\delta t} \Big|_{t-\Delta t}$  to predict  $\mathbf{u}(t + \Delta t)$ , thereby integrating historical derivative information. This key distinction differentiates Adams-Euler from forward Euler, even though both methods produce identical model outputs,  $\frac{\mathbf{u}(t+\Delta t) - \mathbf{u}(t)}{\Delta t}$ .

## 2.2. Proposal of adaptive multi-step rollout

### 2.2.1. Motivation for multi-step rollout

Conventional AR models trained with the loss function of single-step prediction often struggle with error accumulation during long-term rollouts. In single-step training, the model learns to predict only one step ahead using ground truth data as input, but during inference, it must use its own predictions as inputs for subsequent steps. This creates a mismatch between training and inference conditions, as the model is never exposed to its own prediction errors during training. As a result, when small errors occur in early predictions, they can compound and amplify over rollout processes, leading to significant deviations from the true trajectory in long-term predictions. This points out the necessity of the proposing technique for aiding the AR models to implement well in the long-term rollout tasks, which is covered in details in Section 2.2.2.

### 2.2.2. Conventional multi-step rollout

The multi-step rollout approach (Fig. 2), proposed by Wu et al. [29], addresses the limitation discussed in Section 2.2.1 by incorporating multiple future time steps into the training process. By training the model to predict several steps ahead while iteratively using its own predictions as inputs, this approach enhances robustness against error accumulation. It aligns the training and inference conditions, enabling the model to adapt to and mitigate its own prediction errors.

Specifically, given input snapshots  $\mathbf{u}(t), \dots, \mathbf{u}(t - (N - 1))$ , the AR framework first predicts  $\hat{\mathbf{u}}(t + 1)$ . The input history is then updated to  $\hat{\mathbf{u}}(t + 1), \dots, \mathbf{u}(t - (N - 2))$ , allowing to predict  $\hat{\mathbf{u}}(t + 2)$ . This iterative process continues for  $M$  steps, producing predictions from  $\hat{\mathbf{u}}(t + 1)$  to  $\hat{\mathbf{u}}(t + M)$  based on the initial input history  $\mathbf{u}(t), \dots, \mathbf{u}(t - (N - 1))$ , without any backpropagation during inference. The predicted future snapshots, from  $\hat{\mathbf{u}}(t + 1)$  to  $\hat{\mathbf{u}}(t + M)$ , are then used to compute the loss: from  $\mathcal{L}_1$  to  $\mathcal{L}_M$ . In the training process, this method minimizes a multi-step loss function, which aggregates losses across all prediction steps. By explicitly optimizing across multiple steps, the model enhances its resilience to compounding errors during inference. Consequently, the multi-step loss function is defined as a weighted sum of individual step losses, expressed as:

$$\mathcal{L}_{\text{multi-step}} = \sum_{i=1}^M w_i \mathcal{L}_i \quad (10)$$

where  $w_i$  represents the weight assigned to the loss at each future time step  $t + i$ . Notably, when  $M = 1$ , this corresponds to the conventional loss without applying the multi-step rollout technique. Backpropagation with respect to  $\mathcal{L}_{\text{multi-step}}$  enables the model to optimize for long-term predictions by accounting for all loss components, from  $\mathcal{L}_1$  to  $\mathcal{L}_M$ .

However, this technique presents two main challenges:

**Disadvantage 1.** While Wu et al. [29] proposed a weighting strategy for each loss term in multi-step rollout, setting  $w_1 = 1$  for the first future step and  $w_i = 0.1$  for subsequent steps, these weights typically require manual adjustment depending on the specific problem at hand. Optimal weight selection typically involves trial and error, as the ideal values can vary significantly across different datasets and problem types. Reckless weight tuning can destabilize training, leading to issues such as overfitting or underfitting, which compromise model stability and generalization. This instability undermines the effectiveness of multi-step rollout methods, rendering them ineffective for reliable predictions.

**Disadvantage 2.** The conventional multi-step rollout considers all future  $M$  steps simultaneously during training. This can complicate optimization, as the model should account for every snapshot in the long-term future prediction process. As a result, the model might struggle to balance short-term and long-term accuracy, particularly in early stages of training when long-term predictions are highly uncertain. In summary, the simultaneous consideration of all  $M$  steps can lead to poor convergence, as errors from long-term predictions dominate, making it harder for the model to achieve stable optimization.

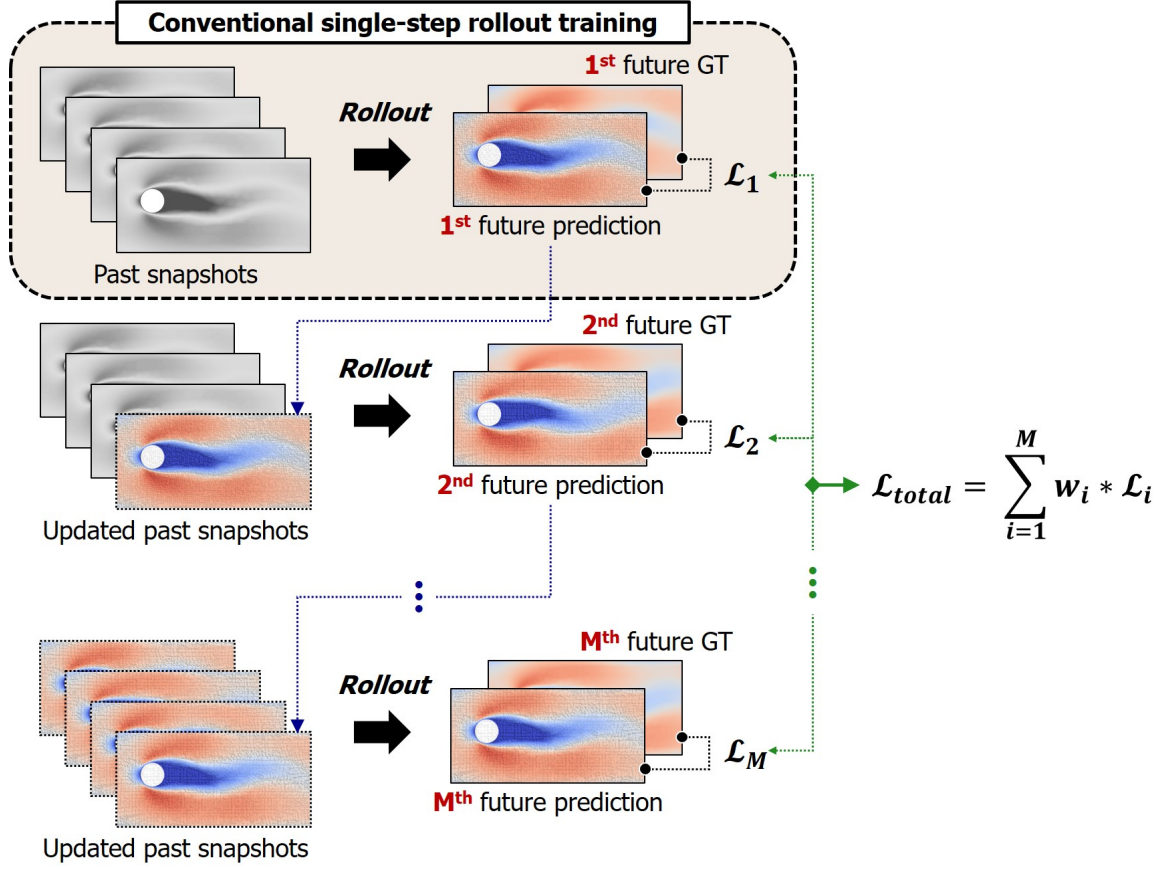


Figure 2: Overview of multi-step rollout: the model predicts  $M$  future steps during training, with the total loss computed as a weighted sum of individual prediction losses at each step. In this study, the adaptive weighting schemes for dynamically determining weights ( $w_i$ ) are newly proposed in Section 2.2.3.

### 2.2.3. Adaptive multi-step rollout

To overcome the limitations of conventional multi-step rollouts, we propose a series of adaptive multi-step rollout strategies designed to enhance training efficiency and improve prediction accuracy over long time horizons, while preserving the scalability of the traditional approach. We introduce three progressively refined ideas to enhance the model’s performance in multi-step predictions. They are named as AW1, AW2, and AW3, where AW refers to the adaptive weighting.

**AW1: adaptive weighting without learnable parameter.** The first approach seeks to mitigate the need for manually selecting weights  $w_i$  by automatically assigning weights based on the magnitude of the prediction errors at each time step. Specifically, the weights are computed as the normalized mean squared error (MSE) for each prediction step:

$$w_i = \frac{\text{MSE}_i}{\sum_{j=1}^M \text{MSE}_j} \quad (11)$$

where  $\text{MSE}_i$  is the MSE at time step  $i$ , and  $M$  is the total number of rollout steps considered in multi-step rollout process. The total loss is then calculated as:

$$\mathcal{L} = \sum_{i=1}^M w_i \cdot \text{MSE}_i \quad (12)$$

This method inherently emphasizes time steps with less accurate predictions, as larger errors yield higher weights. However, because the weights are simply proportional to each MSE value, the approach may lack flexibility in adjusting the importance of different time steps, potentially limiting the model’s capacity to prioritize the most challenging predictions.

---

**Algorithm 1** AW1: adaptive weighting without learnable parameter

---

**Require:** Model  $\mathcal{M}$ , input data  $\mathbf{u}(t), \dots, \mathbf{u}(t - (N - 1))$ , ground truth  $\mathbf{u}(t + 1), \dots, \mathbf{u}(t + M)$

**Ensure:** Updated model parameters

- 1: **for** each training iteration **do**
- 2:     Perform  $M$ -step rollout predictions recursively:

$$\begin{aligned}\hat{\mathbf{u}}(t + 1) &= \mathcal{M}(\mathbf{u}(t), \dots, \mathbf{u}(t - (N - 1))) \\ \hat{\mathbf{u}}(t + 2) &= \mathcal{M}(\hat{\mathbf{u}}(t + 1), \dots, \mathbf{u}(t - (N - 2))) \\ &\vdots \\ \hat{\mathbf{u}}(t + M) &= \mathcal{M}(\hat{\mathbf{u}}(t + M - 1), \dots, \mathbf{u}(t))\end{aligned}$$

- 3:     Compute MSE for each step:

$$\text{MSE}_i = \text{MSE}(\hat{\mathbf{u}}(t + i), \mathbf{u}(t + i)), \quad i = 1, \dots, M$$

- 4:     Compute adaptive weights:

$$w_i = \frac{\text{MSE}_i}{\sum_{j=1}^M \text{MSE}_j}$$

- 5:     Calculate total loss:

$$\mathcal{L} = \sum_{i=1}^M w_i \cdot \text{MSE}_i$$

- 6:     Update model parameters via backpropagation of  $\mathcal{L}$
- 7: **end for**

- 8: **return** Updated model parameters
- 

**AW2: adaptive weighting with learnable parameter.** To introduce more flexibility in adjusting the importance of different time steps, we extend the first idea by incorporating a learnable parameter  $k$  that dynamically adjusts the weighting scheme. The adaptive weights are computed using a power function of the MSE values, modulated by the effective parameter  $k_e$ :

$$w_i = \frac{\text{MSE}_i^{k_e}}{\sum_{j=1}^M \text{MSE}_j^{k_e}} \quad (13)$$

where  $k_e$  is defined as:

$$k_e = 0.5 + 2.5 \cdot \sigma(sk) \quad (14)$$

Here,  $\sigma$  represents a sigmoid activation function, used to bound the value of  $k_e$  within the range of 0.5 to 3. The parameter  $k$  is learnable, and  $s$  acts as a scaling factor ( $s = 10$  is adopted in this study). By learning  $k$  during training, the model can adjust the weighting more flexibly than AW1, depending on what minimizes the total loss:

$$\mathcal{L} = \sum_{i=1}^M w_i \cdot \text{MSE}_i \quad (15)$$



---

**Algorithm 2** AW2: adaptive weighting with learnable parameter

---

**Require:** Model  $\mathcal{M}$ , input data  $\mathbf{u}(t), \dots, \mathbf{u}(t - N + 1)$ , ground truth  $\mathbf{u}(t + 1), \dots, \mathbf{u}(t + M)$

**Ensure:** Updated model parameters and learnable parameter  $k$

- 1: Initialize learnable parameter  $k$
- 2: **for** each training iteration **do**
- 3:     Perform  $M$ -step rollout predictions recursively:

$$\begin{aligned}\hat{\mathbf{u}}(t + 1) &= \mathcal{M}(\mathbf{u}(t), \dots, \mathbf{u}(t - (N - 1))) \\ \hat{\mathbf{u}}(t + 2) &= \mathcal{M}(\hat{\mathbf{u}}(t + 1), \dots, \mathbf{u}(t - (N - 2))) \\ &\vdots \\ \hat{\mathbf{u}}(t + M) &= \mathcal{M}(\hat{\mathbf{u}}(t + M - 1), \dots, \mathbf{u}(t))\end{aligned}$$

- 4:     Compute MSE for each step:  $\text{MSE}_i = \text{MSE}(\hat{\mathbf{u}}(t + i), \mathbf{u}(t + i))$  for  $i = 1, \dots, M$
- 5:     Calculate  $k_e = 0.5 + 2.5 \cdot \text{sigmoid}(sk)$
- 6:     Compute adaptive weights:

$$w_i = \frac{\text{MSE}_i^{k_e}}{\sum_{j=1}^M \text{MSE}_j^{k_e}}$$

- 7:     Calculate total loss:  $\mathcal{L} = \sum_{i=1}^M w_i \cdot \text{MSE}_i$
- 8:     Update model parameters and learnable parameter  $k$  through backpropagation of  $\mathcal{L}$
- 9: **end for**

10: **return** Updated model parameters and  $k$

---

**AW3: simplified adaptive weighting focusing on first and last steps.** Recognizing that errors often accumulate over time in AR predictions, we propose a simplified version of the second idea (AW2) that only considers the losses on the first and last steps of the rollout. Specifically, the total loss is computed using only the MSE at the first step ( $\text{MSE}_1$ ) and the final step ( $\text{MSE}_M$ ), ignoring the losses at intermediate steps. In this situation, the adaptive weights are computed as:

$$\begin{aligned}w_1 &= \frac{\text{MSE}_1^{k_e}}{\text{MSE}_1^{k_e} + \text{MSE}_M^{k_e}}, \\ w_M &= \frac{\text{MSE}_M^{k_e}}{\text{MSE}_1^{k_e} + \text{MSE}_M^{k_e}}\end{aligned}\tag{16}$$

where the two weights are summed to 1. By focusing on the first and last steps, this method emphasizes improving both the immediate next prediction and the long-term prediction, which are critical for model performance. This simplified approach reduces computational complexity and avoids potential overfitting to intermediate steps, while still leveraging the adaptability introduced by the learnable parameter  $k$ .

Finally, the progression from the first to the third approaches for the adaptive weighting can be summarized as below:

- **AW1** introduces automatic weighting based on MSE, providing simplicity but with limited flexibility due to the absence of additional parameters.
- **AW2** incorporates a learnable parameter that flexibly adjusts the weighting scheme.
- **AW3** simplifies the AW2 method by focusing on the most critical steps (first and last), reducing complexity while retaining the benefits of adaptivity.

### 3. Details of the experiments to evaluate spatio-temporal AR prediction performance

In this section, we outline the training process of the Graph U-Net models [30, 24] designed for spatio-temporal flow prediction, specifically applied to the vortex shedding phenomenon behind a two-dimensional (2D) circular cylinder. This specific adoption of a GNN-based model aims to evaluate the performance of our AR framework within a mesh-agnostic SciML paradigm.

#### 3.1. Dataset and preprocessing

The dataset features a mesh scenario with a cylinder placed in a fluid flow, generating vortex shedding characterized by oscillatory flow patterns. The training mesh consists of 1,946 nodes, 11,208 edges, and 3,658 volume cells, as shown in Fig. 3. The flow conditions include a maximum inlet velocity of 1.78, m/s with a parabolic velocity distribution and a cylinder diameter of 0.074, m. A single vortex shedding period comprises approximately 29 snapshots, each capturing the flow field at a specific time step. The training dataset is adapted from the work of Google DeepMind [22]; for further details, please refer to their study.

For training, we utilize only 50 consecutive  $x$ -velocity snapshots from the dataset. Specifically, the model input consists of a sequence of  $N = 20$  past  $x$ -velocity snapshots, fewer than the number of snapshots in a vortex shedding period, forming a 20-channel input graph. The task is to predict the flow field of the next immediate snapshot, enabling the model to learn temporal dependencies within the limited training data.

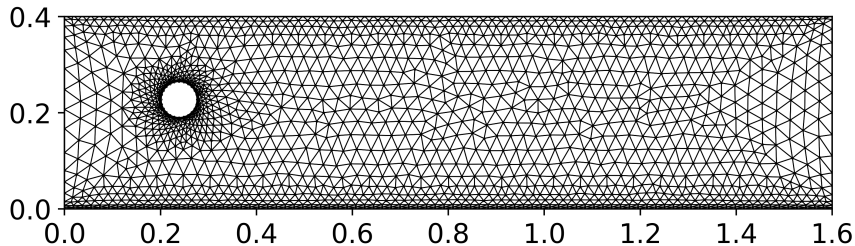


Figure 3: Mesh used for training, containing 1,946 nodes, 11,208 edges, and 3,658 volume cells. The flow is from left to right.

#### 3.2. Model architecture

The Graph U-Net architecture employed in this study is designed with a focus on computational efficiency and simplicity, comprising only 1,177 trainable parameters (Fig. 4). The encoder part of the model consists of four graph convolutional network (GCN) layers [31] with channel dimensions decreasing from 20 to 1 in the sequence 20, 15, 10, 5, and 1. A pooling ratio of 0.6 is applied using the gPool layer [30] after each GCN layer in the encoder, as this ratio was found to be optimal in our previous work [24]. This pooling operation reduces the number of nodes by 60% at each step, effectively capturing multi-scale features while maintaining computational tractability.

The decoder mirrors the encoder with four GCN layers, each having a channel dimension of 1. Skip-connections between corresponding layers of the encoder and decoder are incorporated to facilitate the flow of information and improve reconstruction accuracy. The unpooling operations restore the graph to its original size, ensuring that the output mesh has the same dimensionality as the input.

#### 3.3. Training procedure

The model is trained for 5,000 epochs using the Adam optimizer with an initial learning rate of  $10^{-3}$ . To ensure robustness and capture variability, each training process is repeated three times under identical settings, with the mean performance metrics presented as experimental results. During training, the MSE between predicted and ground-truth snapshots serves as the loss function.

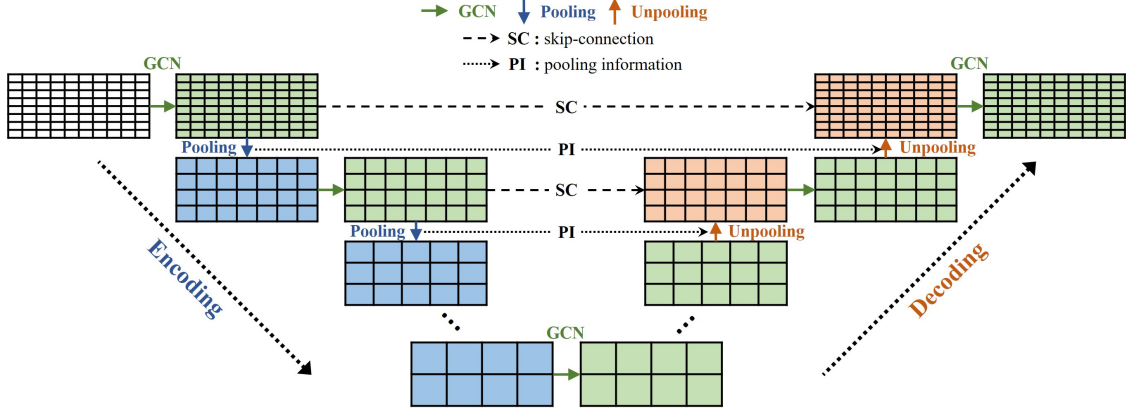


Figure 4: The Graph U-Net architecture consists of an encoder and a decoder, with skip connections facilitating the transfer of information from the encoder to the decoder.

### 3.4. Evaluation and rollout process

After training, the model is evaluated on its ability to predict 350 future snapshots in an AR rollout manner. In each rollout step, the model uses the most recent 20 snapshots to predict the next snapshot. This process is repeated iteratively to generate long-term predictions over the 350-snapshot horizon.

The performance of the model is assessed using the averaged MSE over all 350 predicted snapshots:

$$\text{MSE} = \frac{1}{S} \sum_{s=1}^S \left( \frac{1}{N} \sum_{n=1}^N (y_{n,s} - \hat{y}_{n,s})^2 \right), \quad (17)$$

where  $\hat{y}_{n,s}$  and  $y_{n,s}$  are the predicted and ground-truth values at node  $n$  for snapshot  $s$ , respectively.  $N$  is the total number of nodes, while  $S$  is the number of future snapshots evaluated during the multi-step rollout, which is set to 350 in this study.

### 3.5. Underlying reason for harsh conditions

The model is evaluated under intentionally harsh conditions, including limited model capacity (1,177 parameters), minimal training data (only 50 snapshots), and a long prediction horizon of 350 future snapshots. These constraints simulate practical engineering scenarios where only small datasets are available and computational infrastructure for model training is limited. This challenging setup rigorously tests the model's robustness and its ability to manage error accumulation over time, particularly for complex temporal patterns like vortex shedding. By evaluating under these conditions, we aim to demonstrate the potential of our approach to develop efficient and accurate AR models for spatio-temporal flow prediction, especially in resource-constrained engineering applications.

## 4. Application of time integration schemes into auto-regressive GNNs

In this section, we present the results of applying the four different time integration schemes, along with the conventional direct prediction approach, as described in Section 2.1.2. The objective is to assess their own impact on the long-term prediction accuracy and stability of the Graph U-Net model before incorporating the multi-step rollout technique (which will be addressed in later sections).

Table 1: Comparison of MSE for different time integration schemes over 350 future snapshots. Training time based on NVIDIA 3090 GPU is also shown.

Time Integration Scheme	MSE	Training time [s]
Direct prediction	<b>0.125</b>	2004
Forward Euler	<b>0.138</b>	1867
Second-order central	65.024	1879
Adams-Euler	<b>0.139</b>	1895

#### 4.1. Predictive performance comparison

We evaluate the performance of each time integration scheme by computing the MSE between the predicted and ground-truth flow fields over the entire spatial domain. The MSE values are averaged over 350 future snapshots, providing a comprehensive assessment of each method’s long-term prediction capability. The results are summarized in Table 1.

As observed in Table 1, the direct prediction (conventional approach), forward Euler, and Adams-Euler schemes yield relatively low MSE values, seemingly having better prediction accuracy. In contrast, the second-order central difference exhibits significantly higher errors. The training time on the NVIDIA GeForce RTX 3090 24GB GPU is also summarized (all of the experiments conducted in this study is based on the same GPU), indicating that the use of different time integration schemes does not significantly affect the time required to train the model.

Among various time integration approaches, Fig. 5 illustrates the predicted snapshots when using the second-order central difference scheme. Four consecutive snapshots after 100 rollouts are shown, revealing a highly oscillatory behavior: snapshots after 100 (Fig. 5a) and 102 (Fig. 5c) rollouts appear similar, while those after 101 (Fig. 5b) and 103 (Fig. 5d) exhibit similar patterns. This alternating pattern persists beyond 100 rollouts (not shown here), reflecting a fundamental limitation of the central difference method. Specifically, the next time step,  $\mathbf{u}(t + \Delta t)$ , depends heavily on  $\mathbf{u}(t - \Delta t)$ , bypassing the intermediate state at  $\mathbf{u}(t)$  (as described in Eq. 6). These results align with established findings that the central difference schemes are generally unsuitable for time integration due to their inherent instability, resulting in oscillatory and non-physical solutions.

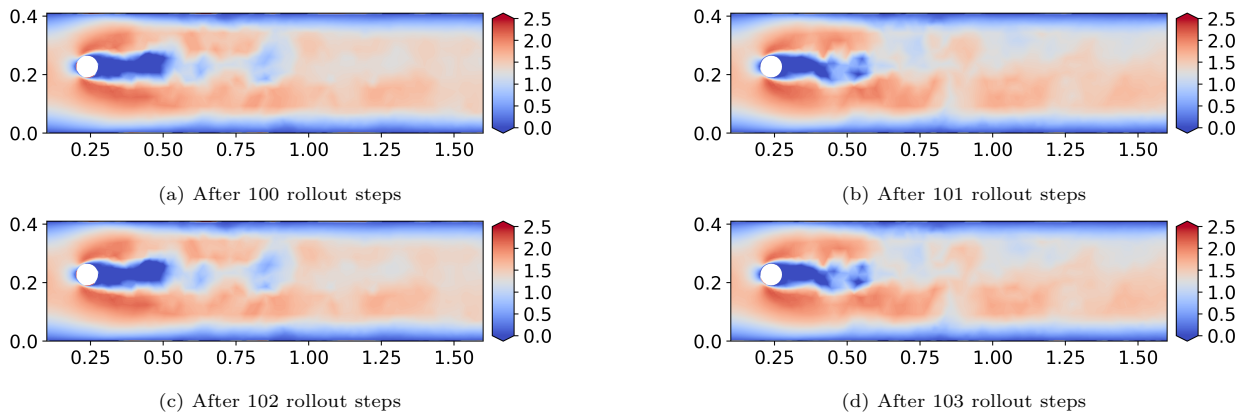


Figure 5: Predicted snapshots using the second-order central difference scheme after (a) 100, (b) 101, (c) 102, and (d) 103 rollout steps. Snapshots after 100 and 102 rollouts display similar patterns, while those after 101 and 103 show similar but alternate patterns.

To further illustrate the performance of the time integration schemes, we visualize the predicted flow fields after 100 rollout steps for selected outperforming schemes: direct prediction, forward Euler, and Adams-Euler. Fig. 6 presents the ground truth flow field and the corresponding predictions and error distributions for selected schemes. Here, the ground truth flow field shows the specific phase during the vortex shedding

pattern behind the cylinder. The predictions from the direct prediction, forward Euler, and Adams-Euler methods show noticeable discrepancies from the ground truth, even after only 100 rollout steps. Especially, in terms of direct prediction, it provides time-averaged results, where the flow fields remain constant as the rollout progresses. The corresponding error plots highlight regions with significant prediction deviations, especially in the wake region where complex flow dynamics are most pronounced.

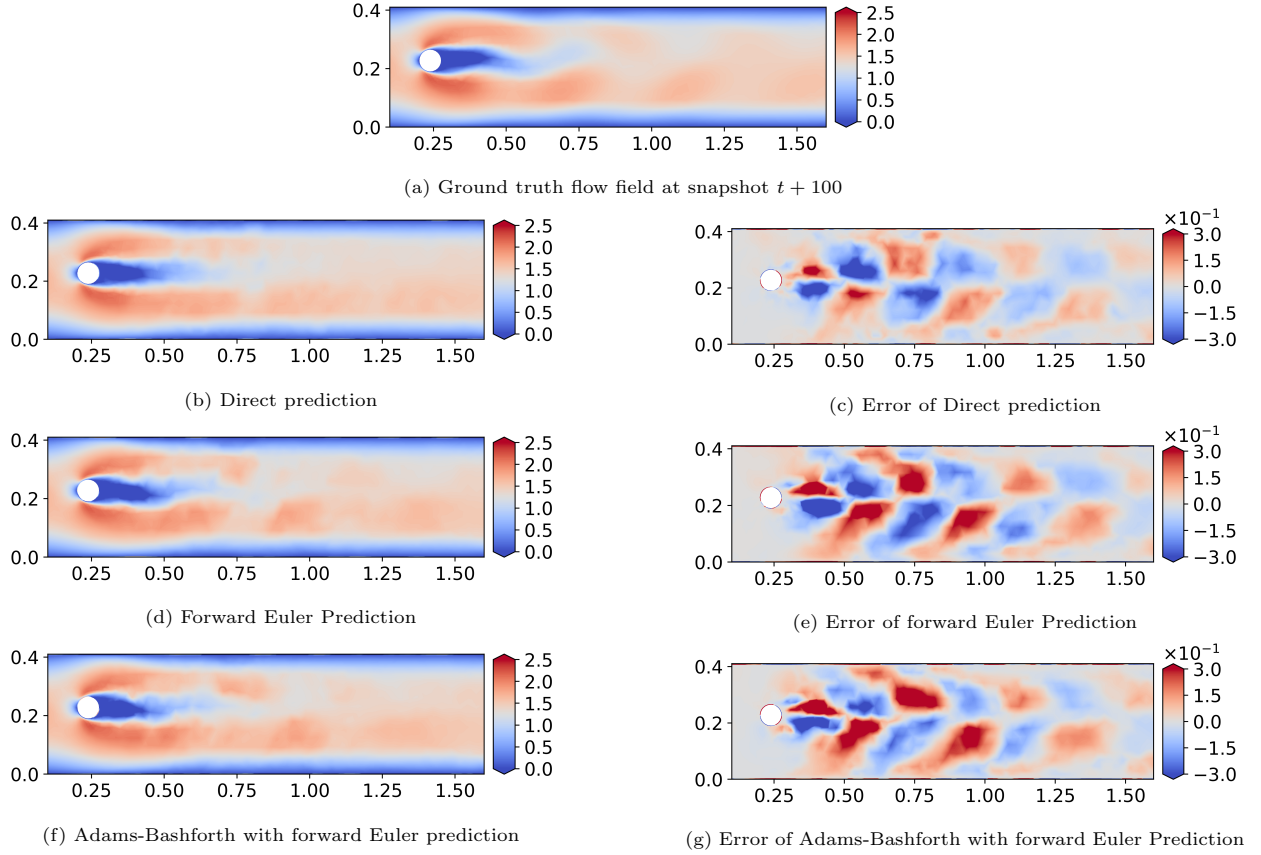


Figure 6: Visualization of the  $x$ -velocity fields after 100 rollout steps. Although only 100 rollout steps are performed, all the time integration methods yield unsatisfactory results.

#### 4.2. Need for additional techniques

The results in Section 4.1 indicate that, despite the relatively low MSE values for some schemes, the Graph U-Net models struggle to maintain accurate long-term predictions over extended rollout horizons. The accumulation of errors becomes apparent even within the first 100 rollout steps, well short of the 350-step prediction horizon that is the main objective of this study. These findings underscore the limitations of directly applying traditional finite difference schemes within AR architectures for time integration, revealing insufficient performance over extended prediction horizons. This highlights the need for enhanced techniques to improve stability and accuracy, such as integrating multi-step rollout strategies to address the observed shortcomings in current methods. In the subsequent sections, we will introduce and evaluate the impact of integrating multi-step rollout techniques with the Graph U-Net models. By combining these approaches with appropriate time integration schemes, we aim to enhance the long-term prediction performance and achieve more reliable forecasts over extended time horizons.

## 5. Extension of time integration schemes into conventional multi-step rollout scenario

In this section, we extend the previously investigated time integration schemes by incorporating conventional multi-step rollout techniques with different values of  $M$ , where  $M$  represents the number of future snapshots considered during training. Specifically, we examine  $M = 1, 2, 4$ , and  $8$ . When  $M = 1$ , it means that the multi-step rollout is not applied, corresponding to the vanilla AR model. By integrating multi-step rollout, we aim to assess whether training the model to predict multiple future steps can enhance long-term prediction accuracy and stability. Note that the conventional weighting strategy suggested by Wu et al. [29] is adopted herein, where the loss weights are set to  $w_1 = 1$  for the first future step and  $w_i = 0.1$  for the subsequent steps in the multi-step rollout (see Eq. 10).

### 5.1. Performance evaluation with conventional multi-step rollout

We evaluate all the time integration schemes with varying values of  $M$  and the MSE results for each combination are presented in Table 2. Here, we can see that increasing the multi-step rollout length  $M$  introduces significant computational overhead, as evidenced by the increased training times from 1,914s ( $M = 1$ ) to 3,131s ( $M = 8$ ) shown in Table 2. However, this increased computational cost does not necessarily lead to improved performance. The results reveal a clear distinction between different time integration schemes: while the Adams-Euler scheme demonstrates consistently robust performance across all values of  $M$  (MSE improving from 0.139 at  $M = 1$  to 0.070 at  $M = 4$ ), other schemes exhibit significant instability. Notably, the direct prediction scheme breaks down completely with NaN errors at  $M = 4$  and  $M = 8$ , while the forward Euler method shows instability at  $M = 2$  (MSE of 581.945) and  $M = 8$  (NaN). Similarly, second-order central difference scheme displays extremely high MSE values across increasing  $M$ .

Table 2: MSE comparison for different time integration schemes with varying multi-step rollout lengths  $M$ . Erroneous values are shown with a gray background.

Time Integration Scheme	Number of considered future snapshots			
	$M = 1$	$M = 2$	$M = 4$	$M = 8$
Direct prediction	0.125	0.102	NaN	NaN
Forward Euler	0.138	581.945	0.075	NaN
Second-order central difference	65.024	1248.223	138.025	0.475
Adams-Euler	0.139	0.092	<b>0.070</b>	0.071
<b>Averaged time [s]</b>	1914	2086	2633	3131

These results reveal two key insights: First, naively increasing  $M$  imposes excessive training constraints on the lightweight model (1,177 parameters), often leading to performance degradation or complete breakdown despite the theoretical benefit of learning longer-term dependencies. Second, the time integration scheme proves more critical than the choice of  $M$ —while most methods fail even with optimal  $M$  values, the Adams-Euler scheme maintains robust performance across all  $M$  values, demonstrating its inherent stability for long-term AR prediction.

**Rationale behind the superior performance of Adams-Euler time integration.** The Adams-Euler-based AR scheme, introduced for the first time in this paper, stands out by maintaining stability even at higher  $M$  values. This superior performance can be attributed to its ability to leverage information from multiple previous time steps—since three successive snapshots,  $\mathbf{u}(t - \Delta t)$ ,  $\mathbf{u}(t)$ , and  $\mathbf{u}(t + \Delta t)$ , are explicitly considered for the prediction of the next snapshot as in Eq. 7—in a mathematically principled way, enabling stable predictions even with limited model capacity.

To illustrate the improved performance achieved with the Adams-Euler scheme with  $M = 4$  multi-step rollout (best case in Table 2), we present visual comparisons of the predicted flow fields after 200 and 300 rollout steps: Fig. 7 shows the ground truth and the model’s predictions at these rollout steps. As seen in Figs. 7a and 7b, the prediction at snapshot  $t + 200$  shows reasonable agreement with the ground truth, capturing the overall flow patterns and vortex shedding behavior at specific phase. This represents

a substantial improvement over the results in Fig. 6, where accurate predictions were unattainable even at 100 rollout steps, clearly demonstrating the effectiveness of combining conventional multi-step rollout with the Adams-Euler scheme.

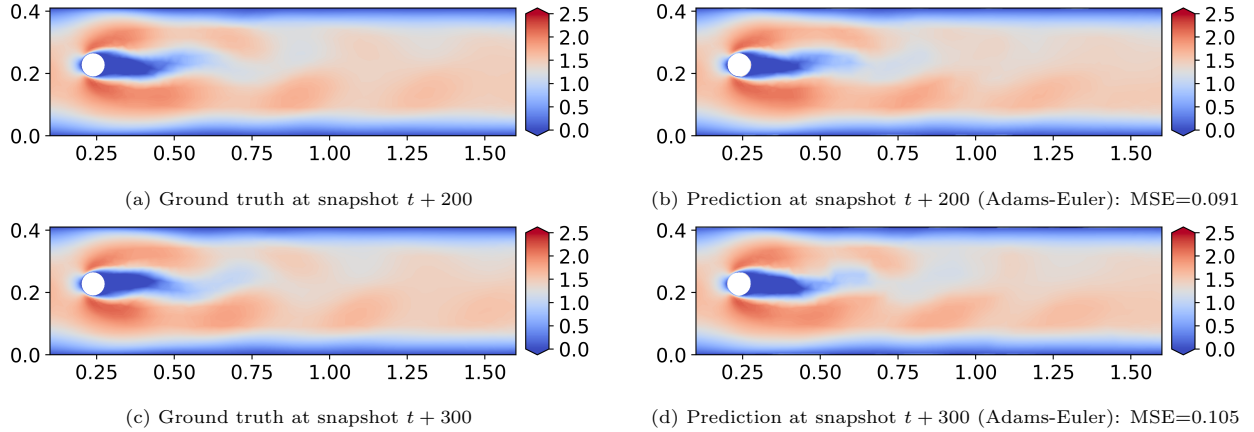


Figure 7: Visualization of the  $x$ -velocity fields at future snapshots using the Adams-Euler scheme with  $M = 4$  multi-step rollout.

However, at snapshot  $t + 300$  (Figs. 7c and 7d), the MSE increases from 0.091 at snapshot  $t + 200$  to 0.105, resulting in a noticeable divergence between the prediction and the ground truth. The accuracy of the flow structures diminishes, with blurred vortex shedding trail. This indicates that while the incorporation of multi-step rollout and the Adams-Euler scheme significantly enhances long-term prediction performance, there remains room for improvement, particularly for prediction horizons extending beyond  $t + 200$ .

## 6. Application of proposed adaptive multi-step rollout

In this section, we evaluate three adaptive multi-step rollout approaches elaborated in Section 2.2.3, aiming to enhance the robustness and accuracy of long-term predictions by automatically adjusting the loss function weights during training.

Performance of the three adaptive weighting strategies across different time integration schemes—direct prediction, forward Euler, and Adams-Euler—is assessed using a more focused evaluation approach. To better evaluate the models’ ability to capture complex wake oscillatory vortex behavior, MSE results from this section are calculated based on  $x$ -velocity data from seven strategic probe points in the wake region (shown in Fig. 8), rather than across the entire field. This targeted analysis provides a more precise assessment of how well each method captures the critical vortex shedding dynamics and the results are summarized in Table 3. For the direct prediction case, while the vanilla approach with fixed weights (MSE of 0.011) outperforms its adaptive variants, it still falls short compared to the best results achieved with forward Euler and Adams-Euler schemes. Notably, both our proposed approaches (AW2 and AW3, which are adaptive weightings with a learnable parameter) demonstrate strong performance with the forward Euler scheme (MSE of 0.007 and 0.010 respectively), which is a widely adopted approach in GNN-based AR prediction. However, the most remarkable performance is achieved by combining the Adams-Euler scheme with AW3, which emphasizes only the first and last loss components during training. This combination yields a significantly lower MSE (0.002) compared to all other methods, establishing it as the optimal approach for long-term prediction in our study. A comparison of the required training time reveals negligible differences across the various weighting approaches: it indicates that the proposed adaptive weighting methods enhance rollout performance without incurring additional computational costs.

To understand how the adaptive weights are adjusted during training in AW2, we visualize the weights assigned to each loss term over epochs for the Adams-Euler scheme as Fig. 9, which reveals two key observations:

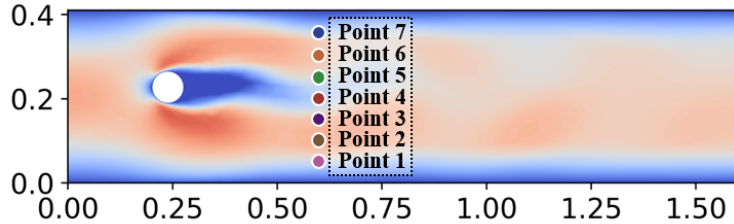


Figure 8: Locations of seven probe points examined to gain a more intuitive and quantitative understanding of vortex shedding prediction performance in terms of  $x$ -velocity.

Table 3: MSE comparison for different adaptive weighting approaches across time integration schemes: multi-step rollout with  $M = 4$  is applied. MSE values here are calculated with respect to seven probe points in Fig. 8.

Time Scheme	Vanilla (fixed weights)	AW1 (without learnable $k$ )	AW2 (with learnable $k$ )	AW3 (first and last only)
Direct prediction	<b>0.011</b>	0.025	0.027	0.027
Forward Euler	0.019	0.023	<b>0.007*</b>	<b>0.010</b>
Adams-Euler	0.018	0.017	<b>0.010</b>	<b>0.002**</b>
<b>Averaged time [s]</b>	2420	2384	2408	2354

\* Model A  
\*\* Model B

- **Stabilization phase (before 1000 epochs):** during the initial training phase, the Graph U-Net stabilizes, with minimal differences observed between the weights of the four loss terms. This indicates that the model is primarily learning basic temporal patterns, while the adaptive weighting mechanism has not yet significantly shifted its focus toward specific time steps.
- **Adaptation phase (after 1000 epochs):** beyond epoch 1000, the weight assigned to the 4th loss term increases relative to the others. The weights for the first three loss terms do not exhibit clear trends or significant differences among themselves.

This trend supports the rationale behind AW3, which focuses on the first and last loss components. The increasing weight of the last loss term indicates that it is more challenging to minimize and is critical to long-term rollout performance—remember that all AW approaches are designed to give more weight to the higher loss term. The lack of distinction among the first three loss terms suggests that emphasizing the first loss term can sufficiently represent the short-term prediction error, allowing the model to allocate more resources to improving long-term accuracy. The corresponding results of the Fig. 9 with respect to the AW3 approach can be found in Fig. B.14 in Appendix B.

To intuitively and quantitatively evaluate the impact of the improvements achieved by AW3 on capturing vortex shedding behavior, we analyze the temporal evolution of the  $x$ -velocity at seven probe points positioned downstream of the cylinder (Fig. 8). Based on these probe points, we compare the predictions of the two best-performing models trained so far (two models with footnotes in Table 3). Model A: the one with forward Euler scheme and AW2 (adaptive weighting with learnable parameter), resulting in an MSE of 0.007. Model B: the other with Adams-Euler scheme with AW3 (first and last loss terms only), resulting in an MSE of 0.002.

Fig. 10 shows the time-series of the  $x$ -velocity at the probe points over 350 future snapshots for both models, along with the ground truth. For Model A (Fig. 10a), the predictions generally capture the vortex shedding patterns, with periodic oscillations similar to the ground truth. However, discrepancies are noticeable, especially at 4th probe point with red colors, where the model fails to accurately reproduce the amplitude and phase of the oscillations. However, in the results of Model B (Fig. 10b), the predictions closely match the ground truth across all probe points, including 4th probe point. The model successfully



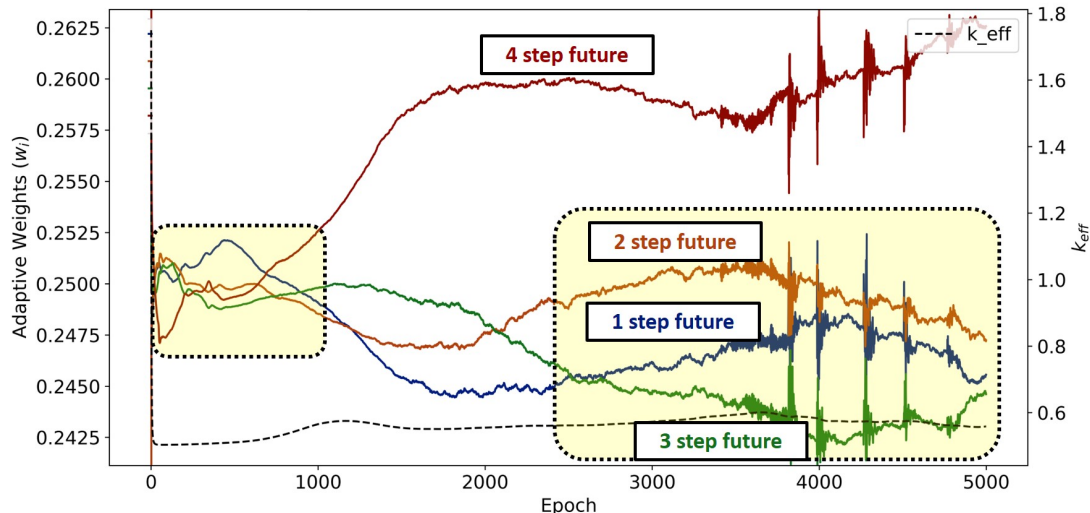


Figure 9: Evolution of adaptive weights for each loss term over epochs in AW2 with the Adams-Euler scheme (multi-step rollout with  $M = 4$ ). Adaptive weights ( $w_i$ ) and effective parameter ( $k_{eff}$ ) are shown in each y-axis.

maintains the correct shedding period and amplitude over the entire prediction horizon, indicating a significant improvement in long-term accuracy. These results demonstrate that focusing on the first and last loss terms during training (AW3) enhances the model’s ability to capture both short-term and long-term temporal dynamics more effectively. This approach yields predictions that are both more accurate and stable compared to AW2, where all loss terms are treated simultaneously.

From Fig. 10b, we have demonstrated successful long-term prediction over 350 rollout steps using an AR Graph U-Net model, despite operating under notably challenging conditions: a severely constrained model capacity (1,177 parameters), minimal training data (50 snapshots), and an extensive prediction horizon (350 rollouts). This achievement can be attributed to two key innovations: (1) the introduction of the Adams-Euler time integration scheme for AR prediction, which provides enhanced numerical stability, and (2) the development of an adaptive weighting strategy that strategically focuses on only the first and last future snapshots during multi-step rollout training.

To further validate the effectiveness of these innovations, the following sections will present two critical comparisons: first, against the conventional noise injection approach widely used for improving long-term AR predictions (Section 7), and second, by testing our model under even more challenging conditions using a truncated mesh domain (Section 8). These comparisons will serve to conclusively demonstrate the robustness and superiority of our proposed methodology.

## 7. Comparison with conventional noise-injection approach for long-term rollout

In this section, we compare the long-term rollout performance of our models against the most widely adopted approach in the field of auto-regression: noise injection [17, 22, 23, 24]. This method deliberately adds random noise to the input data during the training phase to enhance the model’s robustness against error accumulation in AR predictions. The underlying principle is that by exposing the model to perturbed input data during training, it becomes more resilient to imperfect data by learning to handle its own flawed predictions when they are fed back as inputs during inference.

We evaluate three model configurations, all trained with Gaussian noise  $\mathcal{N}(0, 0.16^2)$  injected into the input data. This noise level, identified as optimal in our previous work on the same dataset [24], is consistently applied during training. Notably, evaluations are conducted without multi-step rollouts. The first model employs the traditional direct prediction approach, the second uses the forward Euler time integration

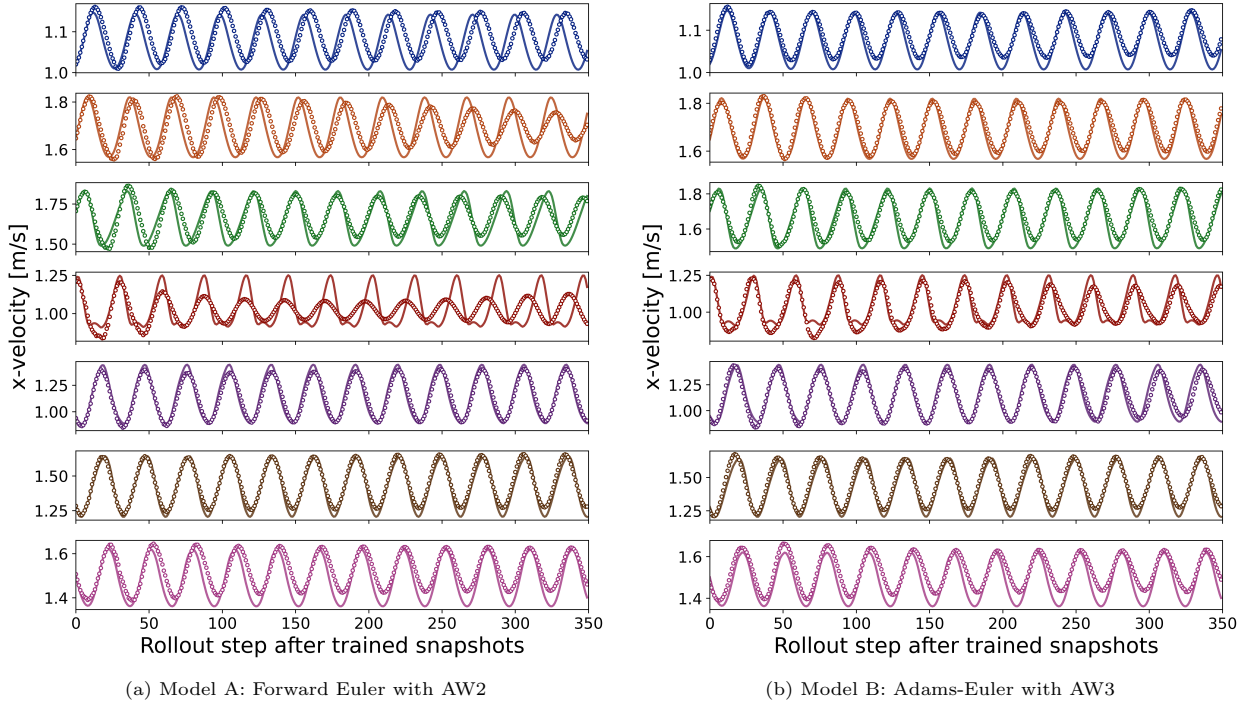


Figure 10: Time series of  $x$ -velocity at the seven probe points over 350 future snapshots: comparison between (a) Model A and (b) Model B. From bottom to top, the plot represents the  $x$ -velocity at probe points 1 through 7 (Fig. 8). Solid lines represent ground truth; circles represent model predictions.

scheme, and the third adopts the Adams-Euler time integration scheme. To assess the effectiveness of noise injection, we again analyze the temporal behavior of the  $x$ -velocity at seven probe points located downstream of the cylinder. Figs. 11a and 11b present the results for models using noise injection with forward Euler and Adams-Euler schemes respectively. For the forward Euler integration scheme, we compare two approaches: adaptive multi-step rollout with AW2 (Fig. 10a) versus noise injection without multi-step rollout (Fig. 11a). The noise injection approach exhibits inferior accuracy at all probe points, with oscillations deviating significantly from ground truth in both amplitude and phase. This indicates that noise injection alone is insufficient to maintain long-term prediction accuracy with forward Euler integration. Similarly, for the Adams-Euler scheme, we compare AW3-based adaptive multi-step rollout (Fig. 10b) versus noise injection without multi-step rollout (Fig. 11b). The noise injection approach again shows less accurate reproduction of vortex shedding patterns, especially for the lower four probe points and after 150 rollout steps.

Notably, when comparing between integration schemes with noise injection (Figs. 11a and 11b), the Adams-Euler method still significantly outperforms forward Euler. This further underscores the robust performance and superior accuracy of the Adams-Bashforth time integration scheme across various training approaches.

To quantify the performance differences, we summarize the MSE with respect to seven probe points for each model configuration in Table 4. The results indicate that, for all time integration schemes, models trained with adaptive multi-step rollout consistently outperform those using noise injection. Specifically, the MSE for the Adams-Euler scheme improves from 0.012 with noise injection to 0.002 with adaptive multi-step rollout—a substantial enhancement in prediction accuracy. Although noise injection improves training efficiency by eliminating the need for additional processing of multiple output snapshots, its cost benefits are surpassed by the superior accuracy achieved with our proposed approach.

The performance gap between adaptive multi-step rollout and noise injection can be attributed to fundamental differences in how these methods address error accumulation. Noise injection attempts to build resilience by introducing input perturbations, making the model more robust to small deviations. However,

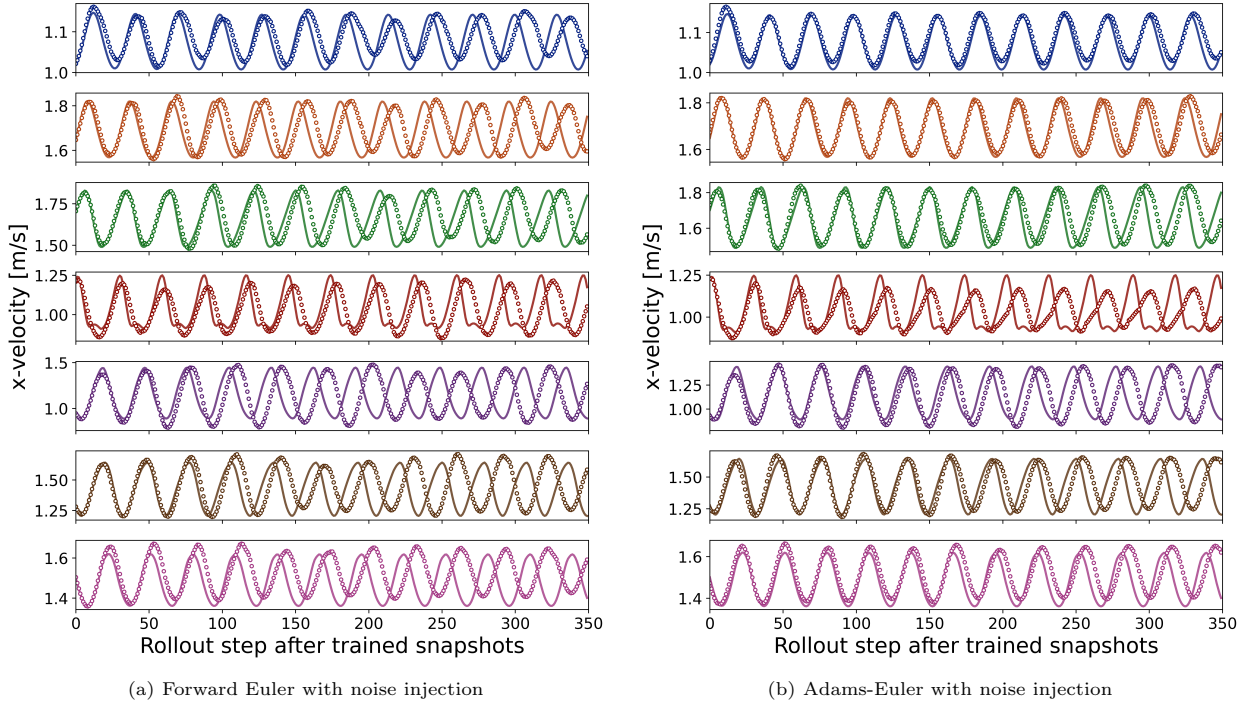


Figure 11: Time series of  $x$ -velocity at probe points over 350 future snapshots using models with noise injection. Solid lines represent ground truth; circles represent model predictions.

Table 4: MSE comparison between adaptive multi-step rollout and noise injection approaches for different time integration schemes. Each time scheme with multi-step rollout utilizes a different adaptive weighting approach for multi-step rollout (as denoted by footnotes), selected as the best configuration for each case. MSE values here are calculated with respect to seven probe points in Fig. 8.

Time Scheme	Multi-Step Rollout	Noise Injection
Direct Prediction	<b>0.011</b> <sup>1</sup>	0.019
Forward Euler	<b>0.007</b> <sup>2</sup>	0.017
Adams-Euler	<b>0.002</b> <sup>3</sup>	0.012
<b>Averaged time [s]</b>	<b>2354</b>	<b>1806</b>

<sup>1</sup> Without adaptive weighting

<sup>2</sup> With AW2

<sup>3</sup> With AW3

this approach does not explicitly address the temporal dependencies and error propagation mechanisms inherent in AR predictions. In contrast, our adaptive multi-step rollout strategy enables the model to learn from multiple future steps simultaneously, using strategically adjusted loss weights to focus on both immediate and distant predictions. The effectiveness of this approach is clearly demonstrated in the time series visualizations, where models trained with adaptive multi-step rollout more accurately capture the vortex shedding patterns compared to those trained with noise injection, as shown in Figs. 10 and 11. These results establish our proposed methodology, combining Adams-Euler time integration with adaptive multi-step rollout, as a more effective and reliable alternative to the traditional noise injection technique for long-term prediction tasks.

*Further investigation: integrating multi-step rollout with noise injection techniques.* Experiments combining multi-step rollout and noise injection were also conducted; however, their performance fell

significantly short compared to methods utilizing either multi-step rollout or noise injection individually. The results suggest that the simultaneous use of these techniques degrades model performance. This degradation occurs because multi-step rollout naturally introduces increasing prediction errors in later future steps while noise injection simultaneously adds artificial perturbations. This combination creates excessive noise that compounds throughout the prediction sequence, making the loss function unstable and preventing effective learning, particularly for distant future predictions.

## 8. Robustness evaluation under more challenging conditions: training with truncated mesh regions

Having achieved successful long-term predictions under stringent conditions—limited datasets, small model capacity, and extensive rollout steps—using the novel integration of the Adams-Bashforth with forward Euler scheme and multi-step rollout with adaptive weighting (Fig. 10b), we further challenge the model’s robustness by evaluating its performance on a truncated mesh. This truncated mesh contains only a portion of the vortex shedding region, specifically defined by the spatial domain  $0.3 < x < 0.75$  and  $0.128 < y < 0.328$ . By focusing on this core region where complex flow dynamics occur, we aim to assess the model’s ability to generalize and maintain accuracy under even challenging conditions.

### 8.1. Experimental setup for truncated mesh scenario

The truncated mesh is a subset of the original computational domain, capturing the essential features of the vortex shedding phenomenon while reducing the spatial extent of the data (region of interest within the flow field is visualized in Fig. 12b~12e). We evaluate the performance of the four models that previously demonstrated satisfactory results, as reported in Table 3: these models include the direct prediction with vanilla multi-step rollout, forward Euler with adaptive weighting approach 2 (AW2), forward Euler with adaptive weighting approach 3 (AW3), and Adams-Euler combined with adaptive weighting approach 3 (AW3).

### 8.2. Results and discussion

Figs. 12b~12e present the predicted flow fields after 300 rollout steps from the four model settings mentioned above, alongside the ground truth in Fig. 12a. We observe that the direct prediction (Fig. 12b) with vanilla multi-step rollout fails to capture the vortex shedding patterns, showing significant deviations from the ground truth. The forward Euler method with AW2 (Fig. 12c) shows some improvement but still struggles to accurately represent the flow structures, especially in the wake region behind the cylinder. The forward Euler method with AW3 (Fig. 12d) and Adams-Euler scheme combined with AW3 (Fig. 12e) closely match the ground truth, successfully reproducing the vortex shedding patterns and flow dynamics within the truncated region. These results highlight the superior performance of the adaptive weighting approach 3 combined with forward Euler or Adams-Euler, even under the harsher condition of a truncated mesh.

To further assess the models’ ability to capture temporal dynamics within the truncated mesh, we analyze the temporal evolution of the  $x$ -velocity at seven probe points strategically located in the wake region, as illustrated in Fig. 13. The results demonstrate clear performance differences across the four model configurations. The direct prediction method (Fig. 13a, MSE: 0.019) completely fails to reproduce the periodic oscillations characteristic of vortex shedding, indicating its fundamental inability to capture flow dynamics in the truncated domain. The forward Euler method with AW2 (Fig. 13b, MSE: 0.011) shows improved performance, successfully capturing the overall oscillatory behavior, though it gradually deviates from the ground truth in both amplitude and phase as the rollout progresses. Similarly, the forward Euler method with AW3 (Fig. 13c, MSE: 0.013) achieves comparable accuracy to AW2 in Fig. 13b, despite of the slightly lower performance. Most notably, the Adams-Euler scheme combined with AW3 (Fig. 13d, MSE: 0.008) demonstrates superior performance, achieving the best agreement with ground truth across nearly all probe points. This configuration accurately captures the vortex shedding frequency, amplitude, and phase throughout the entire prediction horizon, with some deviations observed at probe point 4 (colored as red).

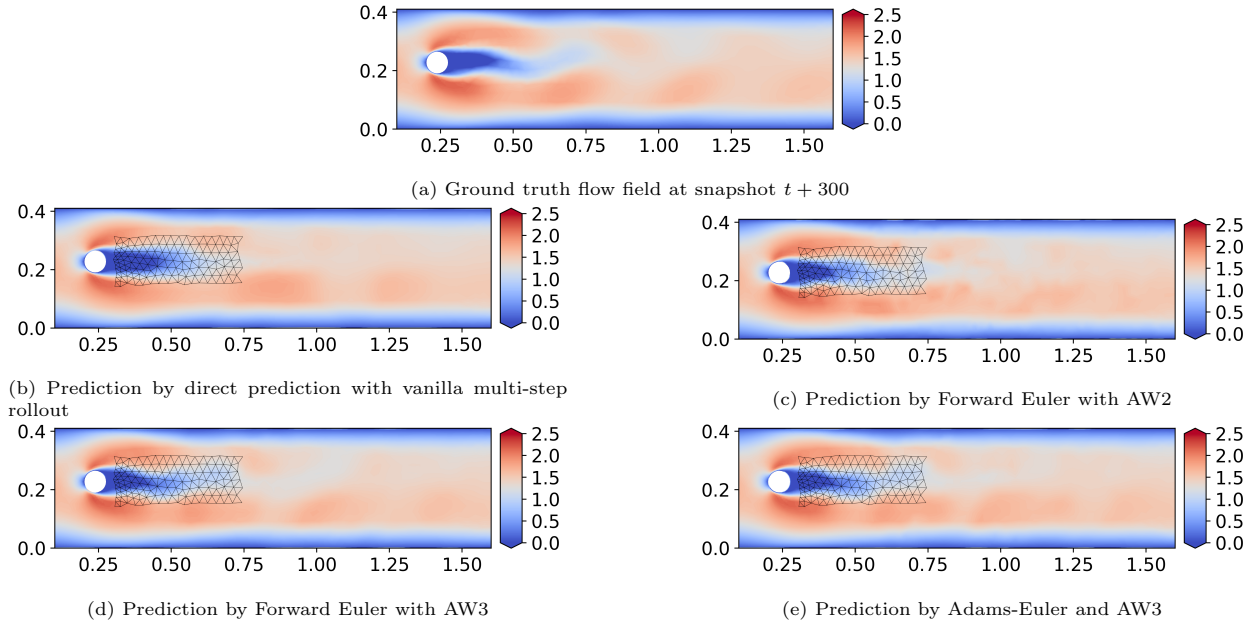


Figure 12: Comparison of predicted  $x$ -velocity fields in the truncated-mesh region after 300 rollout steps. Note that only the part of the mesh shown in the figures was used for training Graph U-Nets.

These results further reinforce the robustness of the Adams-Euler scheme with adaptive multi-step rollout, under the challenging mesh conditions.

### 8.3. Final remarks on the proposed framework: Adams-Bashforth-based adaptive multi-step rollout

The evaluation on a truncated mesh demonstrates the exceptional robustness of our combined Adams-Bashforth with forward Euler scheme and adaptive weighting approach 3, which consistently outperforms alternative methods despite the challenge of predicting flow dynamics with reduced spatial information. While direct prediction and forward Euler methods struggle in this scenario, our integrated approach maintains high accuracy and stability, highlighting the crucial role of appropriate time integration schemes paired with effective training strategies in developing robust autoregressive models. This performance under challenging conditions beyond our previous experiments confirms the broad applicability of our methodology, making it particularly valuable for practical engineering applications where data availability is limited or analysis must focus on specific regions within complex flow fields due to memory constraints.

## 9. Conclusions and future work

This study presents a comprehensive framework for enhancing long-term auto-regressive predictions in SciML models through novel numerical time-integration schemes and adaptive multi-step rollout techniques. By combining the two-step Adams-Bashforth scheme with adaptive rollout strategies, our remarkably lightweight GNN-based model—containing only 1,177 trainable parameters—demonstrates exceptional effectiveness under harsh constraints, achieving accurate predictions of complex dynamics across 350 time steps with only 1.6% error. Despite its minimal computational footprint, our methodology delivers substantial improvements: Adams-Bashforth shows 7% better accuracy over conventional methods, our adaptive strategies provide up to 89% improvement over fixed-weight approaches, and our combined approach outperforms noise injection by 83%, maintaining robustness even on truncated meshes. This powerful yet resource-efficient framework is designed to be model-agnostic, ensuring these advancements can benefit diverse scientific domains without specialized adaptations.

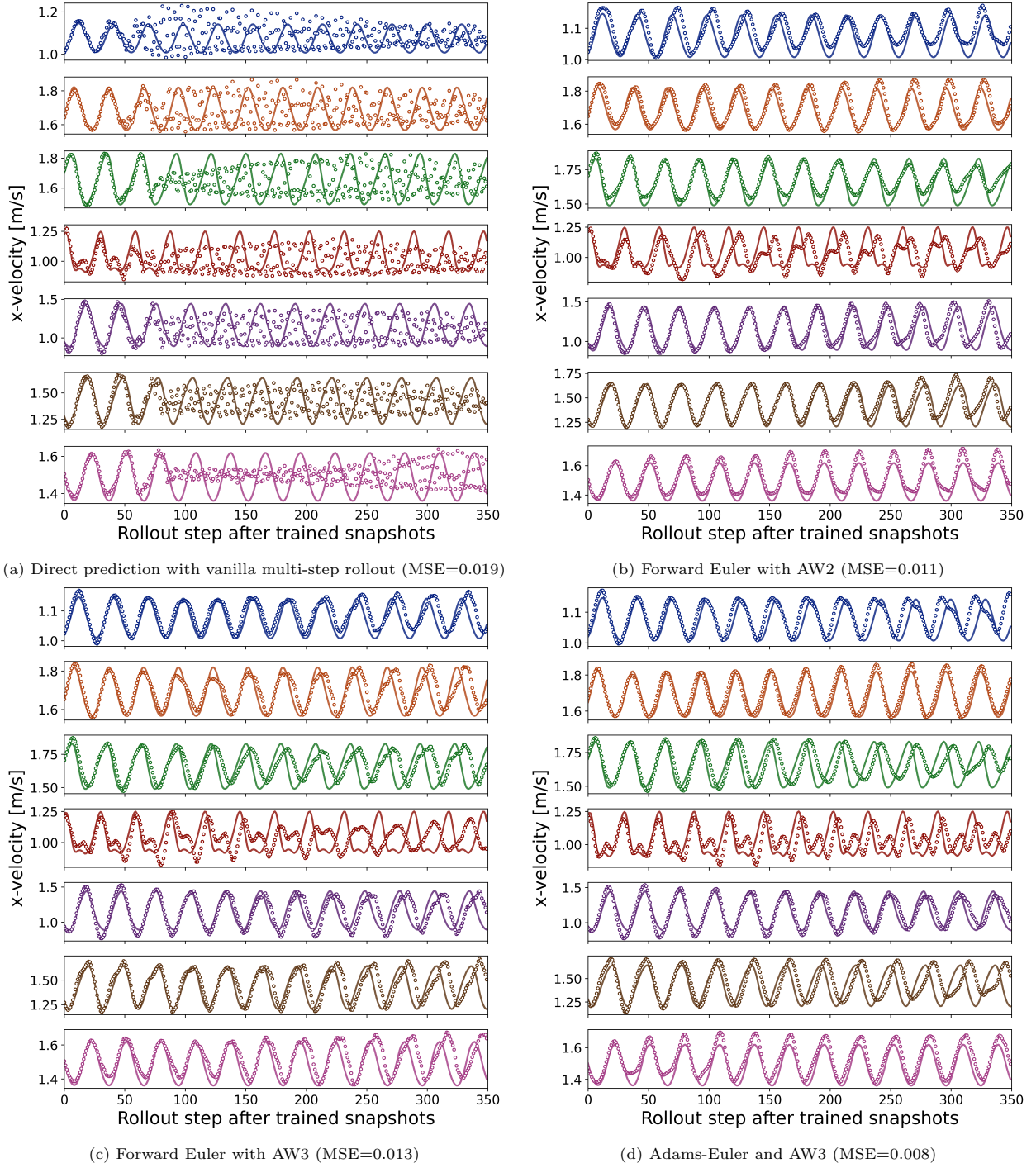


Figure 13: Time series of  $x$ -velocity at probe points over 350 future snapshots for different models trained on truncated meshes. Solid lines represent ground truth; circles represent model predictions.

While our study marks significant advances in AR prediction capabilities, several opportunities for future research remain. First, integrating more advanced higher-order time integration schemes could further improve prediction stability and accuracy. Second, as multi-step rollout involves computing gradients across

multiple future steps, developing more efficient and tactical approaches to reduce its computational overhead would be a valuable direction. Third, incorporating physical principles from the Navier-Stokes equations directly into our framework could enhance both accuracy and physical consistency of predictions, potentially reducing the need for extensive data [32]. Finally, extending the application of our framework to other scientific domains and exploring its performance with diverse neural network architectures and temporal dynamics would provide deeper insights into its broader utility and potential limitations, paving the way for more versatile and scalable solutions.

## Acknowledgments

This work was supported by the National Research Foundation of Korea (2018R1A5A7025409), and the Ministry of Science and ICT of Korea grant (No. 2022-0-00969, No. 2022-0-00986, and No. RS-2024-00355857), the Ministry of Trade, Industry & Energy grant (RS-2024-00410810), and the National Research Council of Science & Technology (NST) grant by the Korea government (MSIT) (No. GTL24031-000). R.V. was supported by ERC Grant No. 2021-CoG-101043998, DEEPCONTROL. The views and opinions expressed are however those of the author(s) only and do not necessarily reflect those of European Union or European Research Council.

## Appendix A. On the applicability of Runge-Kutta methods for AR prediction

While Runge-Kutta (RK) methods [33, 34], particularly the fourth-order scheme, are widely used in numerical integration due to their superior accuracy, their application to AR prediction presents fundamental challenges that make them impractical for our framework. This section illustrates why RK methods were not explored in our study despite their popularity in traditional numerical integration.

### Appendix A.1. Theoretical background of RK

The classic fourth-order Runge-Kutta (RK4) method for solving  $dy/dt = \mathbf{f}(t, \mathbf{u})$  requires four evaluations per time step:

$$k_1 = \mathbf{f}(t, \mathbf{u}(t)) \tag{A.1}$$

$$k_2 = \mathbf{f}(t + \Delta t/2, \mathbf{u}(t) + (\Delta t/2)k_1) \tag{A.2}$$

$$k_3 = \mathbf{f}(t + \Delta t/2, \mathbf{u}(t) + (\Delta t/2)k_2) \tag{A.3}$$

$$k_4 = \mathbf{f}(t + \Delta t, \mathbf{u}(t) + \Delta t k_3) \tag{A.4}$$

The solution is then advanced using:

$$\mathbf{u}(t + \Delta t) = \mathbf{u}(t) + \frac{\Delta t}{6}(k_1 + 2k_2 + 2k_3 + k_4) \tag{A.5}$$

### Appendix A.2. Fundamental challenges of RK in AR context

Although end-to-end training frameworks can, in principle, avoid the need for explicit supervision of intermediate stages, several critical issues make RK methods impractical for AR prediction in our framework.

#### Appendix A.2.1. Intermediate state availability

RK methods inherently rely on intermediate states (e.g.,  $k_2$  and  $k_3$ ), which are evaluated at fractional time steps (e.g.,  $t + \Delta t/2$ ). In typical spatio-temporal datasets used for AR prediction, only full time-step data is available. Even if the network is trained end-to-end using only the final state, this approach undermines the original strength of the RK method. The RK4 algorithm is fundamentally based on a multi-stage time integration process that sequentially leverages previous  $k$  values to accurately capture the dynamics of the system. When end-to-end training is used to mimic the RK property, the intermediate stages are not explicitly supervised or constrained by physical reasons. Consequently, the network merely

combines four model outputs ( $k_1$  through  $k_4$ ) without truly reflecting the underlying multi-stage integration mechanism that is essential to RK methods. This unnecessary implementation not only fails to provide the high-accuracy benefits inherent to the RK approach but also adds complexity without following the original principles of physically motivated time integration.

#### *Appendix A.2.2. Error propagation*

AR prediction inherently suffers from error accumulation, where small prediction errors compound over time as the model uses its own predictions as inputs for subsequent steps. The integration of RK methods would significantly exacerbate this fundamental limitation through a multi-stage compound effect:

- Initial errors in  $k_1$  prediction affect the computation of intermediate state for  $k_2$
- These amplified errors then propagate to  $k_3$  computation through another intermediate state
- Errors further accumulate in  $k_4$  calculation using the previous error-affected states
- All these cascaded errors combine in the final state prediction, which then feeds into the next AR step

This creates a “double cascade” of errors: first through the RK stages within each time step, and then through the AR prediction chain across time steps. While traditional RK methods are designed to reduce numerical integration errors in classical differential equations, their multi-stage nature paradoxically amplifies the inherent error accumulation problem in AR prediction. This dual error amplification makes the training process inherently unstable and potentially divergent, rendering RK methods impractical for AR applications despite their popularity in CFD domain.

#### *Appendix A.2.3. Computational considerations*

While it is true that the RK4 method employs the same function  $\mathbf{f}$  across its four sub-steps, the inputs and corresponding outputs for these evaluations differ significantly. Specifically, the intermediate states  $k_1$ ,  $k_2$ ,  $k_3$ , and  $k_4$  are computed at different time points and with different state inputs. These differences imply that each evaluation essentially encounters a distinct distribution of inputs and produces outputs with different error characteristics. Consequently, even if one were to use a single neural network to represent  $\mathbf{f}$ , the network would need to generalize accurately across these varied sub-tasks—an extremely challenging requirement in practice. Therefore, the RK4 method would require four separate model evaluations per time step, significantly increasing computational cost compared to our adopted Adams-Bashforth scheme. This increased cost is particularly problematic in the context of long-term predictions where hundreds of time steps may be required.

#### *Appendix A.3. Contrast with Adams-Bashforth scheme*

The Adams-Bashforth scheme, as implemented in our work, avoids these challenges by:

- Requiring only directly computable derivatives
- Utilizing historical information rather than intermediate states
- Needing only one model evaluation per time step

#### *Appendix A.4. Conclusion and implications for AR prediction*

While RK methods offer high accuracy in traditional numerical integration, they inherently rely on intermediate states evaluated at fractional time steps that are typically unavailable in AR prediction datasets. Although end-to-end training could approximate RK behavior, this approach fundamentally undermines RK’s strength by combining four model outputs without truly reflecting the physically motivated multi-stage integration mechanism essential to these methods. This implementation adds unnecessary complexity without delivering RK’s accuracy benefits. Our work therefore prioritizes the Adams-Bashforth scheme as a more practical and robust alternative for long-term AR prediction, effectively leveraging available data while maintaining stability and computational efficiency for reliable extended time horizon predictions. Future research might explore hybrid approaches that successfully integrate multi-stage methods while preserving their physical principles within neural network architectures.



## Appendix B. Evolution of the weights in AW3-based multi-step rollout

In Section 6, the weights for each loss term in the AW2-based multi-step rollout are visualized in Fig. 9. This section extends that analysis by presenting results from the AW3-based approach, using the same model configuration as in Fig. 9 but applying AW3 instead of AW2. Fig. B.14 illustrates these results, revealing that after 1,000 epochs, the model begins to stabilize the weights of the first and last future steps, with the last time-step weight slightly exceeding that of the first. This suggests that AW3, which initially considers both the first and last time-step losses, remains highly effective by gradually shifting its focus to the last time step, ensuring greater accuracy in long-term rollouts.

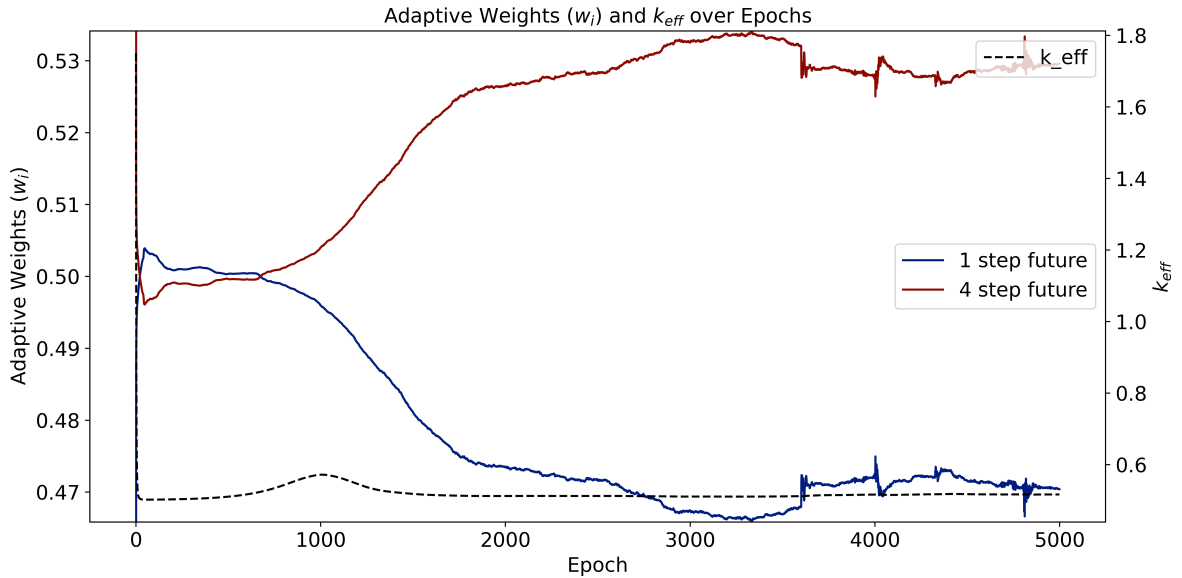


Figure B.14: Evolution of adaptive weights for each loss term over epochs in AW3 with the Adams-Euler scheme.

## References

- [1] A. Solera-Rico, C. Sanmiguel Vila, M. Gómez-López, Y. Wang, A. Almashjary, S. T. Dawson, R. Vinuesa,  $\beta$ -variational autoencoders and transformers for reduced-order modelling of fluid flows, *Nature Communications* 15 (2024) 1361.
- [2] X.-Y. Liu, M. Zhu, L. Lu, H. Sun, J.-X. Wang, Multi-resolution partial differential equations preserved learning framework for spatiotemporal dynamics, *Communications Physics* 7 (2024) 31.
- [3] K. Hasegawa, K. Fukami, T. Murata, K. Fukagata, Cnn-lstm based reduced order modeling of two-dimensional unsteady flows around a circular cylinder at different reynolds numbers, *Fluid Dynamics Research* 52 (2020) 065501.
- [4] S. Lee, D. You, Data-driven prediction of unsteady flow over a circular cylinder using deep learning, *Journal of Fluid Mechanics* 879 (2019) 217–254.
- [5] B. List, L.-W. Chen, K. Bali, N. Thuerey, Differentiability in unrolled training of neural physics simulators on transient dynamics, *Computer Methods in Applied Mechanics and Engineering* 433 (2025) 117441.
- [6] D. Akhare, T. Luo, J.-X. Wang, Physics-integrated neural differentiable (pindiff) model for composites manufacturing, *Computer Methods in Applied Mechanics and Engineering* 406 (2023) 115902.
- [7] S. B. Taieb, G. Bontempi, A. F. Atiya, A. Sorjamaa, A review and comparison of strategies for multi-step ahead time series forecasting based on the nm5 forecasting competition, *Expert systems with applications* 39 (2012) 7067–7083.
- [8] I. K. Ahani, M. Salari, A. Shadman, Statistical models for multi-step-ahead forecasting of fine particulate matter in urban areas, *Atmospheric Pollution Research* 10 (2019) 689–700.
- [9] K. K. R. Samal, K. S. Babu, S. K. Das, Multi-output spatio-temporal air pollution forecasting using neural network approach, *Applied Soft Computing* 126 (2022) 109316.
- [10] H. Wang, Z. Zheng, C. Ji, L. J. Guo, Automated multi-layer optical design via deep reinforcement learning, *Machine Learning: Science and Technology* 2 (2021) 025013.
- [11] B. R. Chang, H. F. Tsai, Forecast approach using neural network adaptation to support vector regression grey model and generalized auto-regressive conditional heteroscedasticity, *Expert systems with applications* 34 (2008) 925–934.

- [12] S. Asadi, A. Tavakoli, S. R. Hejazi, A new hybrid for improvement of auto-regressive integrated moving average models applying particle swarm optimization, *Expert Systems with Applications* 39 (2012) 5332–5337.
- [13] S. Wang, S. Sankaran, P. Perdikaris, Respecting causality for training physics-informed neural networks, *Computer Methods in Applied Mechanics and Engineering* 421 (2024) 116813.
- [14] L. Liu, K. Nath, W. Cai, A causality-deeponet for causal responses of linear dynamical systems, *arXiv preprint arXiv:2209.08397* (2022).
- [15] T. X. Nghiem, T. Nguyen, B. T. Nguyen, L. Nguyen, Causal deep operator networks for data-driven modeling of dynamical systems, in: *2023 IEEE International Conference on Systems, Man, and Cybernetics (SMC)*, IEEE, 2023, pp. 1136–1141.
- [16] A. Venkatraman, M. Hebert, J. Bagnell, Improving multi-step prediction of learned time series models, in: *Proceedings of the AAAI Conference on Artificial Intelligence*, volume 29, 2015.
- [17] J. Kim, J. Park, N. Kim, Y. Yu, K. Chang, C.-S. Woo, S. Yang, N. Kang, Physics-constrained graph neural networks for spatio-temporal prediction of drop impact on oled display panels, *Expert Systems with Applications* (2025) 126907.
- [18] X. Zhang, J. Liu, C. Chen, L. Wei, Z. Wu, W. Dai, Goal-driven long-term marine vessel trajectory prediction with a memory-enhanced network, *Expert Systems with Applications* 263 (2025) 125715.
- [19] H. Gao, X. Han, X. Fan, L. Sun, L.-P. Liu, L. Duan, J.-X. Wang, Bayesian conditional diffusion models for versatile spatiotemporal turbulence generation, *Computer Methods in Applied Mechanics and Engineering* 427 (2024) 117023.
- [20] J. Jeon, J. Lee, S. J. Kim, Finite volume method network for the acceleration of unsteady computational fluid dynamics: Non-reacting and reacting flows, *International Journal of Energy Research* 46 (2022) 10770–10795.
- [21] J. Jeon, J. Lee, R. Vinuesa, S. J. Kim, Residual-based physics-informed transfer learning: A hybrid method for accelerating long-term cfd simulations via deep learning, *International Journal of Heat and Mass Transfer* 220 (2024) 124900.
- [22] T. Pfaff, M. Fortunato, A. Sanchez-Gonzalez, P. W. Battaglia, Learning mesh-based simulation with graph networks, *arXiv preprint arXiv:2010.03409* (2020).
- [23] A. Sanchez-Gonzalez, J. Godwin, T. Pfaff, R. Ying, J. Leskovec, P. Battaglia, Learning to simulate complex physics with graph networks, in: *International conference on machine learning*, PMLR, 2020, pp. 8459–8468.
- [24] S. Yang, R. Vinuesa, N. Kang, Enhancing graph u-nets for mesh-agnostic spatio-temporal flow prediction, *arXiv preprint arXiv:2406.03789* (2024).
- [25] S. Yin, S. Hu, Y. Wang, Y.-H. Yang, High-order adams network (hian) for image dehazing, *Applied Soft Computing* 139 (2023) 110204.
- [26] C. R. Da Cunha, N. Aoki, D. K. Ferry, Y.-C. Lai, A method for finding the background potential of quantum devices from scanning gate microscopy data using machine learning, *Machine Learning: Science and Technology* 3 (2022) 025013.
- [27] K. Hashimoto, K. Matsuo, M. Murata, G. Ogiwara, D. Takeda, Machine-learning emergent spacetime from linear response in future tabletop quantum gravity experiments, *Machine Learning: Science and Technology* (2025).
- [28] R. Das, Application of genetic algorithm for unknown parameter estimations in cylindrical fin, *Applied soft computing* 12 (2012) 3369–3378.
- [29] T. Wu, Q. Wang, Y. Zhang, R. Ying, K. Cao, R. Susic, R. Jalali, H. Hamam, M. Maucec, J. Leskovec, Learning large-scale subsurface simulations with a hybrid graph network simulator, in: *Proceedings of the 28th ACM SIGKDD Conference on Knowledge Discovery and Data Mining*, 2022, pp. 4184–4194.
- [30] H. Gao, S. Ji, Graph u-nets, in: *international conference on machine learning*, PMLR, 2019, pp. 2083–2092.
- [31] F. Ogoke, K. Meidani, A. Hashemi, A. B. Farimani, Graph convolutional networks applied to unstructured flow field data, *Machine Learning: Science and Technology* 2 (2021) 045020.
- [32] S. Yang, H. Kim, Y. Hong, K. Yee, R. Maulik, N. Kang, Data-driven physics-informed neural networks: A digital twin perspective, *Computer Methods in Applied Mechanics and Engineering* 428 (2024) 117075.
- [33] C. Dawson, C. J. Trahan, E. J. Kubatko, J. J. Westerink, A parallel local timestepping runge–kutta discontinuous galerkin method with applications to coastal ocean modeling, *Computer Methods in Applied Mechanics and Engineering* 259 (2013) 154–165.
- [34] T. Arbogast, C.-S. Huang, X. Zhao, D. N. King, A third order, implicit, finite volume, adaptive runge–kutta weno scheme for advection–diffusion equations, *Computer Methods in Applied Mechanics and Engineering* 368 (2020) 113155.